





Magnetic properties of permalloy antidot array fabricated by interference lithography

Cite as: AIP Advances **9**, 035136 (2019); <https://doi.org/10.1063/1.5080111>

Submitted: 05 November 2018 . Accepted: 22 January 2019 . Published Online: 18 March 2019

A. S. Silva , A. Hierro-Rodriguez, S. A. Bunyaev, G. N. Kakazei , O. V. Dobrovolskiy , C. Redondo, R. Morales, H. Crespo, and D. Navas 



View Online



Export Citation



CrossMark

ARTICLES YOU MAY BE INTERESTED IN

[The design and verification of MuMax3](#)

AIP Advances **4**, 107133 (2014); <https://doi.org/10.1063/1.4899186>

[Ferromagnetic resonance linewidth in metallic thin films: Comparison of measurement methods](#)

Journal of Applied Physics **99**, 093909 (2006); <https://doi.org/10.1063/1.2197087>

[High write endurance up to \$10^{12}\$ cycles in a spin current-type magnetic memory array](#)

AIP Advances **9**, 035236 (2019); <https://doi.org/10.1063/1.5079917>

AVS Quantum Science

Co-published with AIP Publishing



Coming Soon!

Magnetic properties of permalloy antidot array fabricated by interference lithography

Cite as: AIP Advances 9, 035136 (2019); doi: 10.1063/1.5080111
Presented: 16 January 2019 • Submitted: 5 November 2018 •
Accepted: 22 January 2019 • Published Online: 18 March 2019



A. S. Silva,¹  A. Hierro-Rodriguez,^{1,2} S. A. Bunyaev,¹ G. N. Kakazei,¹  O. V. Dobrovolskiy,³  C. Redondo,⁴
R. Morales,^{5,6} H. Crespo,¹ and D. Navas^{1,a)} 

AFFILIATIONS

¹IFIMUP-IN/Department of Physics and Astronomy, University of Porto, 4169-007 Porto, Portugal

²SUPA, School of Physics and Astronomy, University of Glasgow, G12 8QQ Glasgow, UK

³Physikalisches Institut, Goethe University, 60438 Frankfurt am Main, Germany

⁴Department of Chemical-Physics, University of the Basque Country UPV/EHU, 48940 Leioa, Spain

⁵Department of Chemical-Physics & BCMaterials, University of the Basque Country UPV/EHU, 48940 Leioa, Spain

⁶IKERBASQUE, Basque Foundation for Science, 48011 Bilbao, Spain

Note: This paper was presented at the 2019 Joint MMM-Intermag Conference.

^{a)}**Corresponding author:** davidnavasotero@gmail.com

ABSTRACT

The magnetic properties of a Permalloy antidot array in square lattice geometry, with circular-rhomboidal hole shape and fabricated by interference laser lithography and ion-beam sputtering have been reported. Magneto-optical Kerr effect magnetometry indicated that the sample exhibits four-fold anisotropic behaviour, i.e. different magnetization loops were observed when the external magnetic field was applied along either x- or y-axis, or along the array diagonal. Broadband ferromagnetic resonance measurements revealed a rich variety of different magnetization configurations in the unsaturated state that can be controlled by the orientation of the external magnetic field. Micromagnetic simulations have been performed to explain the observed results. On the contrary, in the saturated regime the system demonstrated almost isotropic magnetic behaviour that improves with external field increase. The obtained results show the potential of interference lithography for the fabrication of large area antidot arrays.

© 2019 Author(s). All article content, except where otherwise noted, is licensed under a Creative Commons Attribution (CC BY) license (<http://creativecommons.org/licenses/by/4.0/>). <https://doi.org/10.1063/1.5080111>

I. INTRODUCTION

With the development of lithographic techniques, preparation and characterization of patterned magnetic nanostructures is now one of the most active areas of research in magnetism. The versatility of fabrication process allows the assembly of nanodevices, such as non-volatile spin-torque magnetic random access memories (STT-MRAM).¹ Besides of industrial applications, patterned magnetic structures are very attractive as model systems to study fundamental physical properties of small magnetic elements. Patterned nanostructures are mostly prepared by e-beam lithography (EBL) technique that uses an electron beam to expose an electron-sensitive resist. However, in case of large area patterning, laser interference lithography (IL),^{2,3} when not as versatile as EBL, is much more cost effective.

Ferromagnetic antidot arrays, thin films with array of holes, are nanostructures with well-defined magnetization pinning centers or defects. It has been demonstrated that their magnetic properties depend on the structure geometry, such as the hole diameter, inter-hole distance and film thickness. These parameters induce periodic demagnetization field distributions that affect the magnetization reversal process by controlling the nucleation and movement of domain walls.⁴⁻⁷

Although antidot arrays were firstly suggested for magnetic data storage,⁸⁻¹¹ their potential applicability was more recently proposed for magneto-optical based devices¹²⁻¹⁴ and 2D magnonic crystals.^{15,16}

In order to implement the antidot based devices into technological applications, a deeper understanding of their related dynamic magnetic response is required. Up to now, the dynamical behavior

of antidots has been investigated as a function of lattice symmetry,¹⁷ hole diameter,^{18,19} hole shape,^{20,21} inter-hole distance,^{22,23} film thickness,²⁴ lattice defects²⁵ and orientation of an external magnetic applied field.^{17,23,26,27} Therefore, it was confirmed that the rich variety of magnetization configurations in antidot arrays provides a feasible way to tune their spin-wave spectra. All these studies were mainly performed on the samples prepared by either EBL or deep ultraviolet lithography.

Here we describe the magnetic properties of a thin Permalloy (Py) antidot array fabricated by IL. On the contrary to well-defined shapes, namely, square, circular, triangular, or diamond shapes (studied in previous publications^{20,21}), the shape of the holes in our sample has a circular-rhomboidal appearance. Despite the hole imperfection, still only one ferromagnetic resonance peak was observed in the saturated state. Below the saturation, several spin-wave modes were observed, similarly to the ones observed in perfectly-defined lithographed antidot arrays.^{17-19,23,26,27}

II. EXPERIMENTAL METHOD

Py antidot arrays have been prepared over few cm² Si substrates with native oxide using IL, ion beam sputtering deposition (IBS) and liftoff techniques. Templates, with controlled feature sizes and periodicities, were obtained by IL. The antireflective coating WIDE-8B (≈ 80 -nm-thick) and a negative resist tone TSMR-IN027 (≈ 200 -nm-thick) were spin-coated onto (100) Si substrates and exposed using a Lloyd's mirror interferometer with a He:Cd laser ($\lambda = 325$ nm) as the light source. After a double exposure, the resist was post-baked at 110°C and developed in AZ726 MIF. Then, 5-nm Ti seed layer, 10-nm-thick Py film, and a 3-nm Ti capping layer were deposited sequentially by IBS at room temperature and with the base pressure below 1×10^{-8} Torr.²⁸ Finally, ferromagnetic antidot arrays were achieved after a liftoff process by immersing the sample in 1-methyl-2pyrrolidinone (NMP) at 120°C.

While the pattern morphology was analyzed by scanning electron microscopy (SEM) and atomic force microscopy (AFM), the static magnetic properties were studied using magneto-optical Kerr effect magnetometer (MOKE). Broadband ferromagnetic resonance (FMR) measurements were carried out at room temperature using a coplanar waveguide (CPW) connected to a vector network analyzer in the frequency range 0.05-20 GHz (see Ref. 29 for details). The sample was rotated on top of the CPW and the dynamic response was acquired for two different orientations between the antidot lattice directions and the H field. In particular, $\Theta = 0^\circ$ (along the 1st neighbors direction) and 45° (along the 2nd neighbors direction) were considered. The chosen coordinate system is schematically illustrated in Figure 1(a).

Finally, and in order to identify the magnetization response of the Py antidot array, 2-Dimensional micromagnetic simulations using MuMax3 software (Version 3.9.1)³⁰ were performed. According to our sample geometrical and magnetic properties, the 10-nm-thick Py antidot array was simulated using 2D periodic boundary conditions (PBC) with an exchange coupling constant $A_{exch} = 13 \times 10^{-7}$ erg/cm and saturation magnetization of $M_{sat} = 810$ emu/cm³. SEM micrographs were used in order to resemble the real shape of the antidots in the simulations. Assuming that the magnetization is thickness homogeneous, cell size was chosen to be $(5 \times 5 \times 10)$ nm³, which was smaller than Py characteristic exchange

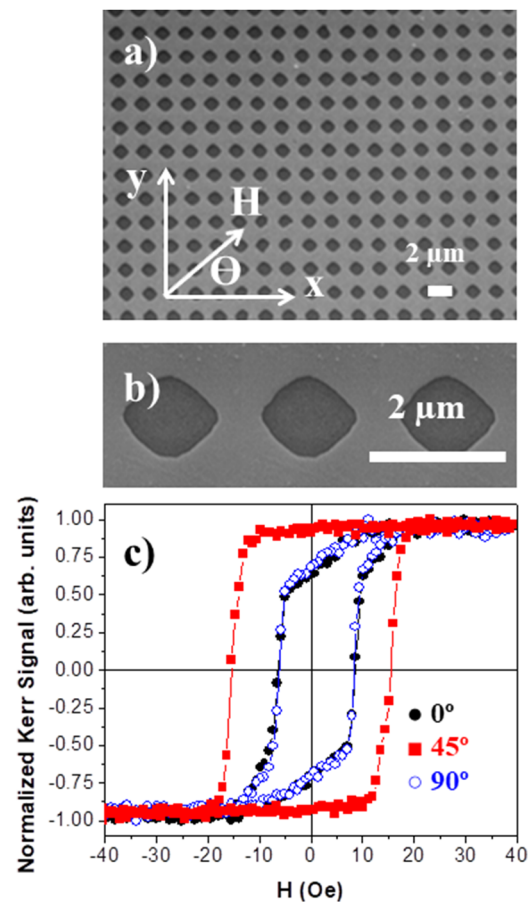


FIG. 1. SEM images (a and b) and hysteresis loops (c) of 10-nm-thick Py antidot array when the external magnetic field was applied along the x-axis ($\Theta = 0^\circ$), y-axis ($\Theta = 90^\circ$) and at 45° ($\Theta = 45^\circ$).

length³¹ (≈ 6 nm). Simulations were performed in a two-step manner: first, hysteresis loops were calculated with the external DC field applied along the two directions experimentally measured (1st and 2nd neighbor directions) with a phenomenological damping of 0.5 to ensure rapid convergence. After this, each of the calculated configurations was excited to extract the dynamic behavior. The excitation used is a modified step function with exponential decay to get a broad frequency range excitation $H_{AC}(t) = h(t - t_0)Ae^{-\alpha(t-t_0)}$. The function h is the step function which is activated after a certain delay time t_0 , A is the pulse amplitude and α is the decay exponential parameter. The excitation pulse was applied in the system plane and perpendicular to the DC field as it was done in the experimental setup. The phenomenological damping for the dynamic simulations was set to 0.01.

III. RESULTS AND DISCUSSION

A. Static analysis

The 10-nm-thick antidot array, with square lattice symmetry, has a periodicity of 2050 nm and hole diameter of 1380 and 1200 nm,

along the x- and y-axis respectively (Figures 1 a and b). Due to the square lattice geometry, the hysteresis loops shows a four-fold anisotropic behavior with similar hysteresis loops when the external magnetic field was applied along the x- ($\Theta = 0^\circ$) and y-axis ($\Theta = 90^\circ$), and an easy magnetization axis at $\Theta = 45^\circ$ (Figure 1 c).

Figure 2 shows the simulated hysteresis loops in combination with snapshots of the magnetization states at different points on the hysteresis curve with the external magnetic field applied along the x-axis, or $\Theta = 0^\circ$, (Figure 2 (a)) and at $\Theta = 45^\circ$ (Figure 2 (b)). The simulated hysteresis loops, like the experimental ones (Figure 1 c), also are different when the external magnetic field is applied along either x- ($\Theta = 0^\circ$) or y-axis ($\Theta = 90^\circ$), and with an easy magnetization axis at $\Theta = 45^\circ$. While the antidot array is well saturated for large applied magnetic fields, different magnetization configurations can be achieved due to the presence of the antidots in the unsaturated states. As soon as the external magnetic field was reduced, holes act as well-defined magnetization pinning centers affecting the

nucleation and movement of domain walls. At remanence, the magnetization snapshot for $\Theta = 0^\circ$ shows two main magnetic domains with magnetization pointed along the x-axis and at 45° . Moreover, an extra magnetic domain, pointed along the y-axis, shows up just before the magnetization switching ($H = -30$ Oe). On the other hand, the magnetization snapshots for $\Theta = 45^\circ$ already show these 3 kinds of domains under an applied field of 25 and 0 Oe. Before the magnetization switching ($H = -50$ Oe), a more complex magnetic configuration is observed.

B. Dynamical behavior

1. Saturated regimen

In the general case, the ferromagnetic resonance frequency of the sample depends significantly on the presence of different anisotropies, particularly magneto-crystalline, surface and field-induced one. However in case of relatively thick (i.e. above few nanometers) polycrystalline soft ferromagnetic film, the contribution of all these anisotropies is negligible, and the FMR frequency is determined by the object shape and can be described by the Kittel equation:³²

$$f_{res} = \frac{\gamma}{2\pi} \sqrt{(H - (N_x - N_y)M_{sat})(H - (N_x - N_z)M_{sat})}, \quad (1)$$

where $\gamma/2\pi$ is the gyromagnetic factor, H is the applied magnetic field, M_{sat} is the saturation magnetization and N_x , N_y , and N_z are the demagnetizing factors along different directions (with z being oriented along the normal to film plane) and $(N_x + N_y + N_z) = 4\pi$.

First, we characterized the 10-nm-thick reference Permalloy film. In the case of a thin film $N_x=N_y=0$, $N_z=4\pi$, and we were able to fit the experimental $f_{res}(H)$ dependence of the FMR resonance peak with $\gamma/2\pi = 2.96$ MHz/Oe and $M_{sat} = 810$ emu/cm³, which are standard parameters for Permalloy.³³ No evidence of in-plane uniaxial anisotropy was found by applying external magnetic field along different directions of the film. The results of this fit were shown in Figure 3 by a blue line.

Although it is impossible to obtain analytical formulas for the demagnetizing factors of an antidot array, particularly with holes of imperfect shape, we could assume that N_x is still equal to N_y . Therefore, Equation (1) can be written as

$$f_{res} = \frac{\gamma}{2\pi} \sqrt{H(H - (N_x - N_z)M_{sat})} \quad (2)$$

Only one sharp FMR peak was observed in the saturated antidot array (Figure 3). Using the same values of gyromagnetic factor and saturation magnetization as for the reference Py continuous film, we obtained $N_z - N_x = 8.6$, that gives $N_x = N_y = 1.32$, $N_z = 9.9$. This clearly indicates how the introduction of holes into the continuous film (in this case the holes occupy approximately 20% of the sample volume) modifies the demagnetizing factors. The FMR-VNA spectra together with respective fits for two external magnetic field H orientations: $\Theta = 0^\circ$ and $\Theta = 45^\circ$ are shown in Figure 3. Although $f_{res}(H)$ experimental dependencies are looking almost identical, a deeper analysis revealed some differences between them. Above some critical field $H_{cr} = 2750$ Oe, both spectra for $\Theta = 0^\circ$ and 45° coincide. Below H_{cr} the difference between two geometries appears, reaching noticeable ≈ 20 Oe for $H = 400$ Oe. This four-fold anisotropy, not expected in uniformly magnetized samples, is explained by the

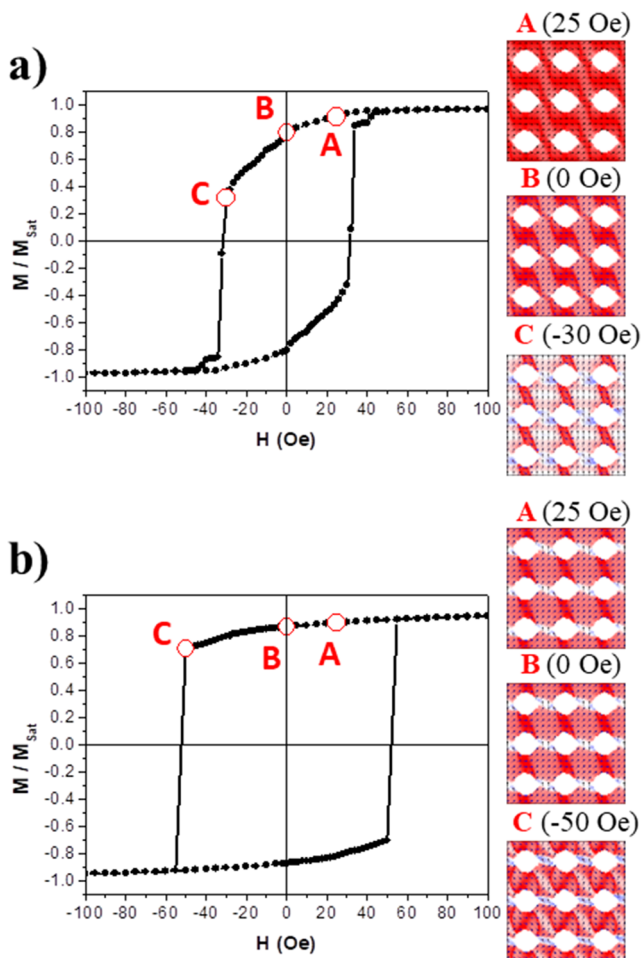


FIG. 2. Simulated hysteresis loops of 10-nm-thick Py antidot array and snapshots of the magnetization when the external magnetic field was applied along the (a) x-axis ($\Theta = 0^\circ$) and (b) at $\Theta = 45^\circ$. The images of the magnetization was recording with different external applied fields (a) A = 25 Oe, B = 0 Oe and C = -30 Oe, and (b) A = 25 Oe, B = 0 Oe and C = -50 Oe.

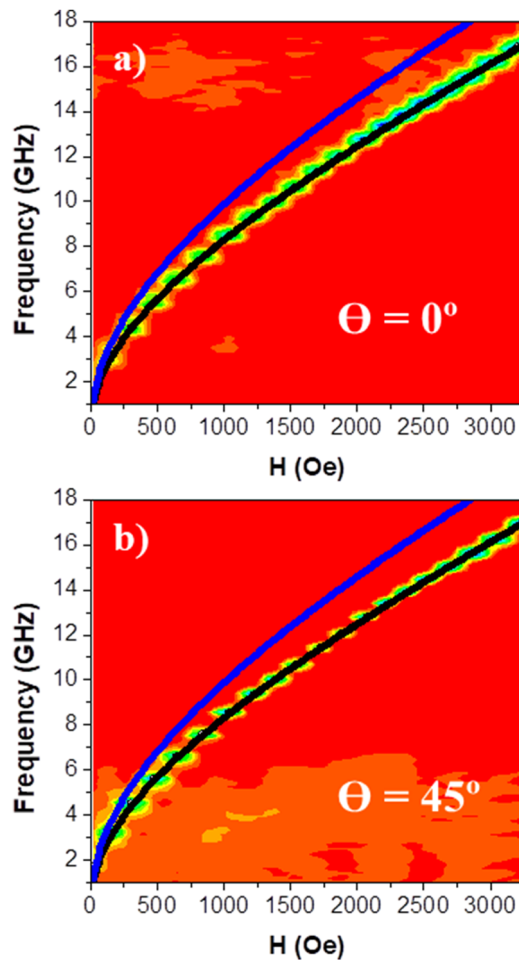


FIG. 3. VNA-FMR spectra of the 10-nm-thick Py antidot array with the external magnetic field applied (a) along the x-axis ($\Theta = 0^\circ$) and (b) $\Theta = 45^\circ$. The black lines correspond to the fits using the Kittel formula (Equation 2); the blue lines correspond to the fit for a 10-nm-thick continuous Py film (spectra not shown).

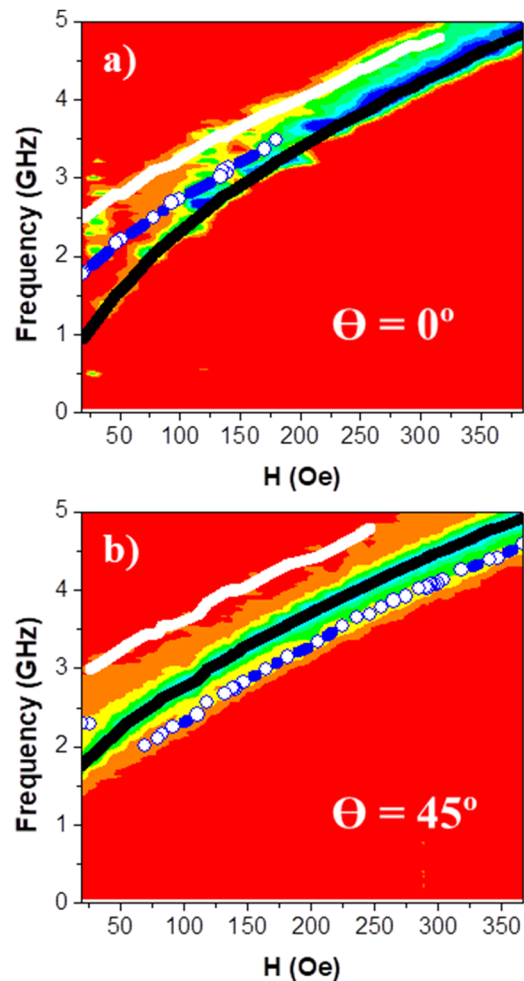


FIG. 4. VNA-FMR spectra of the 10-nm-thick Py antidot array in the unsaturated regime and when the external magnetic field was applied along the x-axis (a) and at $\Theta = 45^\circ$ (b). While the black lines correspond to the main resonance peaks, the white line and empty blue circles correspond to the second and third soft modes.

fact that below a critical field, the magnetization inside the antidot array is non-uniform and the level of non-uniformity depends on the direction of the external magnetic field (being lower for $\Theta = 45^\circ$). This effect was previously observed in closely packed square Py dot arrays.³⁴

2. Unsaturated regimen

As in the unsaturated regime a rich variety of magnetization configurations were observed (Figure 2), different dynamic responses were also obtained at $\Theta = 0^\circ$ and 45° (Figure 4). Up to three resonance peaks, one main peak plus two extra soft ones, were observed at low applied magnetic fields. This peak splitting at low fields has been already described in the bibliography and it was associated to different magnetization arrangements.^{17-19,23,26,27}

As the FMR condition for a ferromagnetic antidot array cannot be described by the Kittel equation any longer in the

unsaturated regime, the micromagnetic simulations have been used to unravel the multi-peaks dynamical spectra. Figure 5 shows the simulated spectra of the 10-nm-thick Py antidot array in the unsaturated regime as well as snapshots of the magnetization states with an applied magnetic field of $H = 25$ Oe.

In order to get a better agreement with the experimental data, we simulated the magnetic field distribution of the Py antidot FMR spectra (Figure 5 a) applying the external magnetic field with a deviation of 5° from the x-axis ($\Theta = 5^\circ$). As it was observed in the experiment, the main resonance peak is accompanied by few extra soft peaks. The simulated magnetization state image at $H = 25$ Oe shows two main regions (A and B). While in region A, the magnetization is parallel to the external applied magnetic field along the x-axis, the magnetic moments are aligned at $\approx 45^\circ$ in region B. As the performed dynamic micromagnetic simulations provide

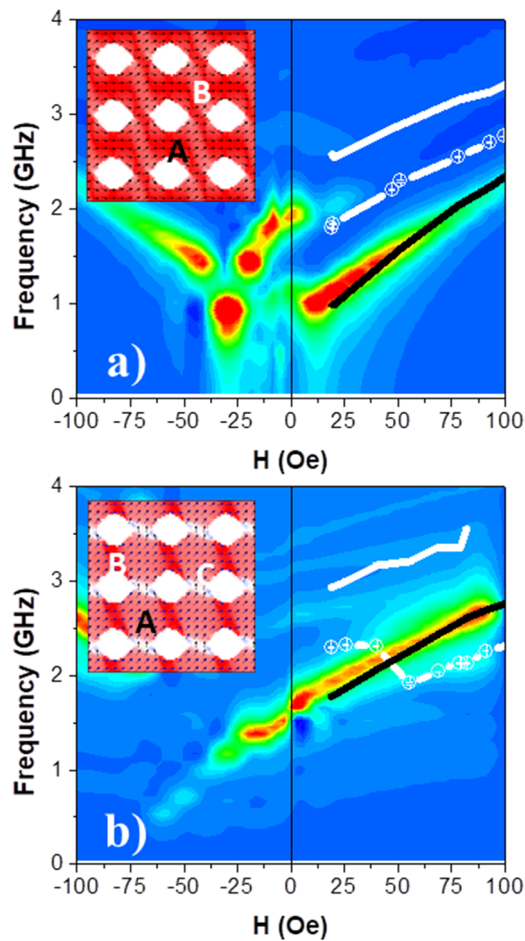


FIG. 5. Experimental resonance peaks (extracted from Figure 4) and simulated VNA-FMR spectra of the 10-nm-thick Py antidot array in the unsaturated regime and when the external magnetic field was applied at $\Theta = 5^\circ$ (a) and $\Theta = 45^\circ$ (b). Moreover, the simulated magnetization states at 25 Oe were shown when the external magnetic field was applied at $\Theta = 0^\circ$ (a) and $\Theta = 45^\circ$ (b).

information related with the average magnetization oscillation amplitude as a function of the frequency and external applied magnetic field, we do not have spatial resolution for the identification of the modes. However, a qualitative analysis can be performed in term of signal contribution. Therefore, the main resonance mode is associated with the larger region A, instead of the soft resonance modes that is linked to region B.

On the other hand, the Py antidot FMR spectra with the external magnetic field applied at $\Theta = 45^\circ$ (Figure 5 b) also show a main resonance peak accompanied by few extra soft peaks. The simulated magnetization state at 25 Oe shows three main regions (A, B and C). While in region A, the magnetization is parallel to the external applied magnetic field ($\Theta = 45^\circ$), the magnetic moments are aligned at $\approx 0^\circ$ and 90° in region B and C, respectively. Again, the main resonance mode is associated with the larger region A, instead of the two soft resonance modes that are linked to regions B and C.

IV. SUMMARY

The evolution of the static and dynamic magnetic properties of a thin Py square antidot lattice with circular-rhomboidal hole shape has been investigated both theoretically and experimentally. The system demonstrates an isotropic magnetic behaviour in the saturated regime. Instead, and in agreement with bibliography,^{17-19,23,26,27} several spin-wave modes were observed in the unsaturated state. Therefore, the obtained results show the potential of IL for the fabrication of large area antidot arrays that can be particularly used as gigahertz-range spin wave filters.

ACKNOWLEDGMENTS

The Portuguese team acknowledges the Network of Extreme Conditions Laboratories-NECL and Portuguese Foundation of Science and Technology (FCT) support through the projects NORTE-01-0145-FEDER-022096, MIT-EXPL/IRA/0012/2017, POCI-01-014 5-FEDER-031302, EXPL/IF/01191/2013 (D.N.), EXPL/IF/00541/2015 (S.A.B.), EXPL/IF/00981/2013 (G.N.K). D.N., G.N.K., C.R and R.M. acknowledge the support by the European Union Horizon 2020 Research and Innovation Programme under Marie Skłodowska-Curie Grant Agreement EU H2020-MSCA-RISE-2016 (No 734801). The Spanish team acknowledges the support from Spanish MINECO through the grant FIS2016-76058 (AEI/FEDER, UE). A.H.-R. acknowledges the support from European Union's Horizon 2020 research and innovation program under the Marie Skłodowska-Curie Action (reference H2020-MSCA-IF-2016-746958). G.N.K. and O.V.D. acknowledge the support from European Cooperation in Science and Technology (COST) project CA16218 "NANOCOBYBRL."

REFERENCES

- S. Bhatti, R. Sbiaa, A. Hirohata, H. Ohno, S. Fukami, and S. N. Piramanayagam, *Materials Today* **20**, 530 (2017).
- T. A. Savas, M. Farhoud, H. I. Smith, M. Hwang, and C. A. Ross, *J. Appl. Phys.* **85**, 6160 (1999).
- C. Lu and R. H. Lipson, *Laser Photonics Rev.* **4**, 568 (2010).
- P. Vavassori, G. Gubbiotti, G. Zangari, C. T. Yu, H. Yin, H. Jiang, and G. J. Mankey, *J. Appl. Phys.* **91**, 7992 (2002).
- C. C. Wang, A. O. Adeyeye, and N. Singh, *Nanotechnology* **17**, 1629 (2006).
- M. Jaafar, D. Navas, A. Asenjo, M. Vázquez, M. Hernández-Vélez, and J. M. García-Martín, *J. Appl. Phys.* **101**, 09F513 (2007).
- N. G. Deshpande, M. S. Seo, X. R. Jin, S. J. Lee, Y. P. Lee, J. Y. Rhee, and K. W. Kim, *Appl. Phys. Lett.* **96**, 122503 (2010).
- R. P. Cowburn, A. O. Adeyeye, and J. A. C. Bland, *J. Magn. Magn. Mater.* **173**, 193 (1997).
- R. P. Cowburn, A. O. Adeyeye, and J. A. C. Bland, *Appl. Phys. Lett.* **70**, 2309 (1997).
- L. Torres, L. Lopez-Diaz, and J. Iñiguez, *Appl. Phys. Lett.* **73**, 3766 (1998).
- M. B. A. Jalil, *J. Appl. Phys.* **93**, 7053 (2003).
- G. Ctistis, E. Papaioannou, P. Patoka, J. Gutek, P. Fumagalli, and M. Giersig, *Nano Lett.* **9**, 1 (2009).
- J. B. González-Díaz, J. M. García-Martín, A. García-Martín, D. Navas, A. Asenjo, M. Vázquez, M. Hernández-Vélez, and G. Armelles, *Appl. Phys. Lett.* **94**, 263101 (2009).
- M. Rollinger, P. Thielen, E. Melander, E. Ostman, V. Kapaklis, B. Obry, M. Cinchetti, A. García-Martín, M. Aeschlimann, and E. Th. Papaioannou, *Nano Lett.* **16**, 2432 (2016).
- S. Neusser and D. Grundler, *Adv. Mater.* **21**, 2927 (2009).

- ¹⁶V. V. Kruglyak, S. O. Demokritov, and D. Grundler, *J. Phys. D: Appl. Phys.* **43**, 264001 (2010).
- ¹⁷S. Tacchi, M. Madami, G. Gubbiotti, G. Carlotti, A. O. Adeyeye, S. Neusser, B. Botters, and D. Grundler, *IEEE Trans. Magn.* **46**, 1440 (2010).
- ¹⁸J. Ding, D. Tripathy, and A. O. Adeyeye, *J. Appl. Phys.* **109**, 07D304 (2011).
- ¹⁹R. Zivieri, P. Malago, L. Giovannini, S. Tacchi, G. Gubbiotti, and A. O. Adeyeye, *J. Phys.: Condens. Matter* **25**, 336002 (2013).
- ²⁰D. H. Y. Tse, S. J. Steinmuller, T. Trypiniotis, D. Anderson, G. A. C. Jones, J. A. C. Bland, and C. H. W. Barnes, *Phys. Rev. B* **79**, 054426 (2009).
- ²¹R. Mandal, P. Laha, K. Das, S. Saha, S. Barman, A. K. Raychaudhuri, and A. Barman, *Appl. Phys. Lett.* **103**, 262410 (2013).
- ²²C. Yu, M. J. Pechan, and G. J. Mankey, *Appl. Phys. Lett.* **83**, 3948 (2003).
- ²³O. N. Martyanov, V. F. Yudanov, R. N. Lee, S. A. Nepijko, H. J. Elmers, R. Hertel, C. M. Schneider, and G. Schönhense, *Phys. Rev. B* **75**, 174429 (2007).
- ²⁴A. Vovk, V. Golub, O. Salyuk, V. N. Krivoruchko, and A. I. Marchenko, *J. Appl. Phys.* **117**, 073903 (2015).
- ²⁵A. Manzin, G. Barrera, F. Celegato, M. Coisson, and P. Tiberto, *Sci. Rep.* **6**, 22004 (2016).
- ²⁶S. Neusser, B. Botters, M. Becherer, D. Schmitt-Landsiedel, and D. Grundler, *Appl. Phys. Lett.* **93**, 122501 (2008).
- ²⁷S. Tacchi, M. Madami, G. Gubbiotti, G. Carlotti, A. O. Adeyeye, S. Neusser, B. Botters, and D. Grundler, *IEEE Trans. Magn.* **46**, 172 (2010).
- ²⁸C. Redondo, S. Moralejo, F. Castaño, W. Lee, K. Nielsch, C. A. Ross, and F. J. Castaño, *Nanotechnology* **17**, 2040–2045 (2006).
- ²⁹M. Tokaç, S. A. Bunyaev, G. N. Kakazei, D. S. Schmool, D. Atkinson, and A. T. Hindmarch, *Phys. Rev. Lett.* **115**, 056601 (2015).
- ³⁰A. Vansteenkiste, J. Leliaert, M. Dvornik, M. Helsen, F. Garcia-Sanchez, and B. Van Waeyenberge, *AIP Adv.* **4**, 107133 (2014).
- ³¹G. S. Abo, Y.-K. Hong, J. Park, J. Lee, W. Lee, and B.-C. Choi, *IEEE Trans. Magn. Mater.* **49**, 4937 (2013).
- ³²C. Kittel, *Phys. Rev.* **73**, 155 (1948).
- ³³G. N. Kakazei, G. R. Aranda, S. A. Bunyaev, V. O. Golub, E. V. Tartakovskaya, A. V. Chumak, A. A. Serga, B. Hillebrands, and K. Y. Guslienko, *Phys. Rev. B* **86**, 054419 (2012).
- ³⁴G. N. Kakazei, Yu. G. Pogorelov, M. D. Costa, T. Mewes, P. E. Wigen, P. C. Hammel, V. O. Golub, T. Okuno, and V. Novosad, *Phys. Rev. B* **74**, 060406 (2006).